

Configurational Entropy of Self Propelled Glass Formers

Sachin C N and Ashwin Joy*

Department of Physics, Indian Institute of Technology Madras, Chennai, Tamil Nadu 600036, India

(Dated: December 13, 2022)

The configurational entropy is an indispensable tool to describe super-cooled liquids near the glass transition. Its calculation requires the enumeration of the basins in the potential energy landscape and when available, it reveals a direct connection with the relaxation time of the liquid. While there are several reports on the measurement of configurational entropy in passive liquids, very little is understood about its role in active liquids which have a propensity to undergo a glass transition at low temperatures. In this paper, we report a careful calculation of the configurational entropy in a model glass former where the constituent units are self propelled. We show that unlike passive liquids, the anharmonic contribution to the glass entropy in these self-propelled liquids can be of the same order as the harmonic contribution, and therefore must be included in the calculation of the configurational entropy. Our extracted configurational entropy is in good agreement with the generalized Adam-Gibbs relation predicted by the random first order transition theory enabling us to deduce a scaling relation between the configurational entropy and the point-to-set length scale in these active systems. Our findings could be of great utility in conventional active systems such as self-propelled granules, Janus particles and dense bacterial suspensions, to mention a few.

I. INTRODUCTION

Active matter systems remain non-equilibrium due to energy conversion at the level of constituent particles that eventually leads to a systematic motion. They span a wide range of physical systems—from bacterial suspensions [1, 2] and ant colonies [3] to even bird flocks [4] and fish schools [5]. The constituent units have their size ranging from a few micrometer to a meter. The effect of self-propulsion results in a plethora of exotic collective behavior whose counterpart is absent in the passive systems [6–11]. Some of these effects can also be witnessed in jamming [12], intermittency [13], non-trivial velocity correlations [14], phase separation [15–17], active liquid meta-materials [18] and even phase transitions [19, 20]. Experimental studies on the living systems have revealed intriguing behavior which resembles the ubiquitous glass transition. For e.g, in the experiment of zebrafish embryonic explants [21], the formation of a cage by the neighboring particles results in short time sub-diffusive behavior that is reminiscent of glassy dynamics. This makes active matter a new paradigm to investigate fundamental issues in glass transition. One of the most debated question in glass physics is how the relaxation time scales diverge as the liquid approaches glass transition temperature? [22, 23]. The random first order transition (RFOT) theory suggests that the relaxation of the liquid occurs through the rearrangement of the correlated mosaics of local domains which are not periodic—the mosaics being the region of unique configurations [24–26]. It also suggests that the driving force for the rearrangements of these correlated regions is the configurational entropy S_c . The extension of RFOT theory on active matter [27, 28] has revealed that the effect of activity on the glassy behavior can be elucidated by study-

ing the microscopic ways in which activity influences S_c . This has resolved the apparent diverging predictions that the effect of activity can either enhance [29] or mitigate [30] the glassy behavior. Though the configurational entropy plays a crucial role in explaining the effect of self-propulsion on the glassy behavior, the detailed simulation studies of the same is sparse in the literature for self-propelled glass formers. While there have been some effort [31] to compute S_c of an active system using an effective temperature approach, its connection with the relaxation dynamics and the size of the cooperatively rearranging regions especially in the vicinity of glass transition, remains to be explored. This is a pressing issue that requires a careful examination of the potential energy landscape (PEL) and its connection to S_c . We aim to bridge this gap by providing a detailed study of how activity influences the movement of the system on this landscape, in turn affecting the configuration entropy S_c and therefore the relaxation dynamics. To achieve this, we start with configurations equilibrated at some effective temperature and self propulsion as input to the energy minimization, to find the local minima of the PEL—referred to as the inherent structures (IS). The multiplicity of these IS directly lead us to an estimate of the configurational entropy that is in very good agreement with the generalized Adam-Gibbs (AG) relationship predicted by the RFOT. Our work reveals that unlike passive liquids, the anharmonic contribution to the glass entropy in these self-propelled liquids can be of the same order as the harmonic contribution, and therefore must be included in any calculation of S_c . Following this we extract a point-to-set (PTS) length scale ξ_s by randomly pinning a fraction of particles in an equilibrated configuration. Finally by invoking a generalized Adam-Gibbs relation, we derive a scaling relation between S_c and ξ_s . We believe these results could be very useful in physical systems such as self-propelled granular systems [32] and active Janus colloidal particles [33] to name a few. The organization

* ashwin@physics.iitm.ac.in

of this paper is as follows, in section II we describe the simulation model used in this study, section III contains the detailed information about the calculation of the configurational entropy, in section IV we have explained the extraction of length scale and its connection to the configurational entropy through RFOT. Finally, in section V, we provide the conclusions of our results.

II. SIMULATION MODEL

In this study, we use a numerical model in which the motion of each active particle is governed by the Ornstein-Uhlenbeck (OU) process. In the overdamped limit, equations of motion for the i^{th} particle is given by

$$\begin{aligned}\dot{\mathbf{r}}_i &= \frac{1}{m\gamma} \left(-\nabla_i U + \mathbf{f}_i \right) \\ \dot{\mathbf{f}}_i &= \frac{1}{\tau_p} \left(-\mathbf{f}_i + \sqrt{2m\gamma k_B T_{\text{eff}}} \boldsymbol{\eta}_i \right)\end{aligned}\quad (1)$$

where U is the interaction potential between the particles in the system that is described later and γ is the friction coefficient. This active OU stochastic process is an athermal model as it lacks the thermal noise and has been extensively used in the studies of athermal active fluids [34–36]. We drop the hydrodynamic interactions in our model as they are decoupled from the glass transition that happens over a much longer time scale. In this model, activity is therefore completely controlled by two

parameters, namely, the effective temperature T_{eff} which sets the strength of the activity and a time scale τ_p , which sets the duration of persistent motion. The active force \mathbf{f}_i has the following time correlation.

$$\langle \mathbf{f}(t) \cdot \mathbf{f}(\mathbf{0}) \rangle = \frac{T_{\text{eff}}}{\tau_p} \exp(-t/\tau_p) \quad (2)$$

The Gaussian white noise has the following statistics-

$$\langle \eta_i^\chi(t) \rangle = 0, \quad \langle \eta_i^\chi(t) \eta_j^\zeta(t') \rangle = \delta_{\chi\zeta} \delta_{ij} \delta(t-t') \quad (3)$$

Here χ, ζ represent spatial indices and i, j denote particle labels. In the limit of $\tau_p \rightarrow 0$, our model described by eq. 1 reduces to the standard overdamped Brownian dynamics that also satisfies the detailed balance [37]. Here the mass of the each particle m , the Boltzmann constant k_B and the friction coefficient γ are all set to unity in all the production runs. The simulation details of our work are as follows. The equations of motion in Eq. 1 is integrated using a fully implicit scheme with a time step of 2×10^{-4} which confirms the numerical stability of the production runs throughout the parameter space [38]. We have employed the Kob-Andersen model in the simulation which is a binary glass forming liquid with 80% large (L) and 20% small (S) particles interacting via the Lennard-Jones (LJ) potential energy [39] at density $\rho = 1.2$. To achieve speed up, we truncated the interaction potential ϕ and its two derivatives at a cut-off distance of r_c .

$$U = \frac{1}{2} \sum_{i \neq j} \phi_{ij}; \quad \phi_{ij} = \begin{cases} 4\epsilon_{ij} \left[\left(\frac{\sigma_{ij}}{r_{ij}} \right)^{12} - \left(\frac{\sigma_{ij}}{r_{ij}} \right)^6 \right], & 0 < r_{ij} \leq r_m \\ \epsilon_{ij} \left[A \left(\frac{\sigma_{ij}}{r_{ij}} \right)^{12} - B \left(\frac{\sigma_{ij}}{r_{ij}} \right)^6 + \sum_{n=0}^3 C_{2n} \left(\frac{r_{ij}}{\sigma_{ij}} \right)^{2n} \right], & r_m < r_{ij} \leq r_c \\ 0, & r_{ij} > r_c \end{cases} \quad (4)$$

The constants A, B, C_0, C_2, C_4 and C_6 are fixed by matching the potential and its two derivatives at the boundaries $r_m = 2^{1/6}\sigma_{ij}$ and the $r_c = 2.5\sigma_{ij}$. The units of length, energy and time are respectively taken as $\epsilon_{LL}, \sigma_{LL}$ and $\sqrt{m\sigma_{LL}^2/\epsilon_{LL}}$. In these units, the values of the potential parameters are set as, $\epsilon_{LL} = 1.0$, $\epsilon_{SS} = 0.50$, $\epsilon_{LS} = 1.50$, $\sigma_{LL} = 1.0$, $\sigma_{SS} = 0.8$. All the simulations were carried out at a fixed volume in a cubic box with 1000 particles. The length of each side in reduced units is taken as 9.41036 and we have used periodic boundary conditions in all the three directions. The range of effective temperatures explored in this paper are $0.45 \leq T_{\text{eff}} \leq 0.9$ and the range of persistence times covered are over three orders of magnitude $2 \times 10^{-4} \leq \tau_p \leq 0.1$. In the following section, we give the details of our calculations of the configurational entropy

in this active system.

III. CONFIGURATIONAL ENTROPY

Conventional phase transitions such as a liquid to crystal transition is accompanied by the emergence of a long range structural order. A super-cooled liquid does not reveal such long range ordering near the glass transition even though its relaxation time increases by several orders of magnitude. This happens because the number of available distinct states in the PEL becomes sub-extensive as the liquid approaches glass transition. The enumeration of these distinct states therefore directly leads to the estimation of S_c . In practice, this is evaluated as the difference between the total and the glass

entropy:

$$S_c = S_{\text{tot}} - S_{\text{glass}} \quad (5)$$

where the total entropy $S_{\text{tot}} = S_{\text{id}} + S_{\text{exc}}$, is calculated by a thermodynamic integration [40, 41]. The glass entropy S_{glass} carries the contribution from the vibrational degrees of freedom and is determined from the PEL. The input to all these calculations are the snapshots at some steady state that is characterized by an effective temperature and a persistence time. These calculations are discussed further in the following sections.

A. Total entropy S_{tot}

This section describes the procedure to compute the total entropy per particle, a sum of the ideal gas entropy S_{id} and the excess entropy S_{exc} . The excess entropy at a given state point can be calculated via thermodynamic integration starting from a reference state where the exact entropy is known [42, 43]. We take the limit $T_{\text{eff}} \rightarrow \infty$ as this reference state which is common practice for such calculations. The total entropy for any soft interaction such as the Lennard-Jones potential then reads as,

$$S_{\text{tot}} = S_{\text{id}} + \beta U(\beta) - \int_0^\beta d\beta' U(\beta') \quad (6)$$

where $U(\beta)$ is potential energy averaged over the ensemble at some inverse effective temperature $\beta = 1/T_{\text{eff}}$. The ideal gas entropy per particle can be evaluated as

$$S_{\text{id}} = \frac{d+2}{2} - \ln \rho - \ln \Lambda^d + S_{\text{mix}} \quad (7)$$

where, d is the spatial dimension, Λ is the thermal wavelength and $S_{\text{mix}} = -\sum_{m=1}^M X_m \ln X_m$ is the mixing entropy per particle. Here X_m are the concentration of m^{th} species. The integral in the Eq. 6 is then evaluated by fitting the averaged potential energy with the Rosenfeld-Tarazona polynomial [44, 45]

$$U(\beta) = a + b\beta^{-k}. \quad (8)$$

Figure 1 shows this numerical fitting with the parameters a , b and k mentioned in table I. Figure 2 shows the variation of S_{tot} as a function of T_{eff} for various τ_p values and it is evident that at a fixed T_{eff} , increasing activity has the effect of increasing total entropy. Later in section III C we show how increasing the persistence time correlates positively with glassy behavior using the arguments of configurational entropy and energy barrier. In the following section we explore the PEL of this system and calculate S_{glass} using the normal modes of vibrations.

τ_p	a	b	k
0.0002	-8.27519	2.42532	0.648819
0.002	-8.3846	2.10334	0.562469
0.02	-9.44373	2.57571	0.240193
0.1	-13.3553	6.13897	0.0627211

TABLE I. Fitting parameters a , b and k for different persistence times that are used in Eq. 8.

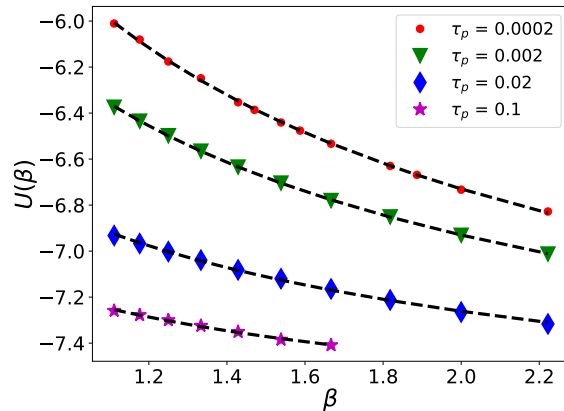


FIG. 1. Temperature dependence of average potential energy at various values of persistence time. Dashed lines indicate fitting to Eq. 8 with parameters listed in table I.

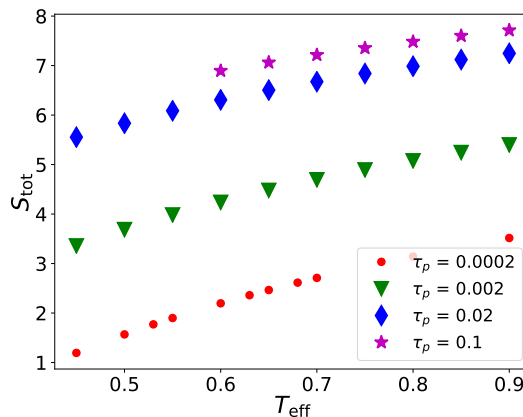


FIG. 2. Total entropy as a function of effective temperature at different values of τ_p . It is increasing as a function of increasing τ_p at any fixed effective temperature.

B. Glass Entropy from Inherent Structures

1. Inherent structures

Inherent structure (IS) is a local minimum of the PEL that can provide important structural information of the glass forming liquids [46–49]. The multiplicity of such structures gives a direct measure of the configurational

entropy. In our work, we used the steady state configurations at a given effective temperature and minimizing their energy using the conjugate gradient method [50, 51]. Figure 3 shows the variation of averaged IS energy $\langle E_{IS} \rangle$ as a function of the effective temperature plotted at various persistence times. It can be observed that at a particular T_{eff} , $\langle E_{IS} \rangle$ becomes negatively larger at large τ_p —implying the system samples deeper minima in the PEL. The harmonic contribution to glass entropy

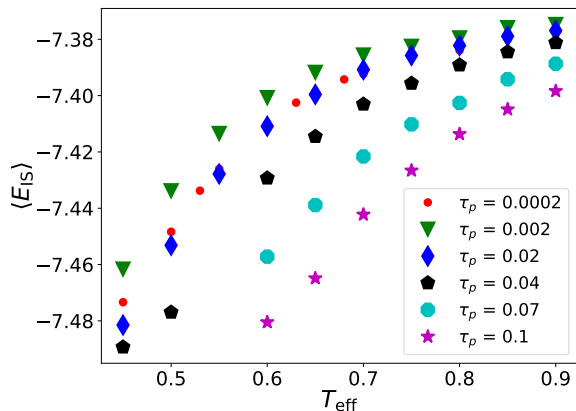


FIG. 3. Temperature dependence of the averaged inherent structure energies at various levels of activity. Here the data is averaged over 200 realizations and the standard deviation is of the order $\sim 10^{-2}$.

$S_{\text{glass}}^{\text{harm}}$ is calculated by making a harmonic approximation to the potential energy close to the IS. This is explained further in the following section.

2. Harmonic contribution to the glass entropy

We start with a typical steady state configuration and quench it to the nearest inherent structure via the conjugate gradient procedure [52]. We then calculate the Hessian of these minimized states, which is a matrix that gives the second derivative of the potential energy [45, 53]

$$\mathcal{H}_{\chi\zeta}^{ij} = \frac{\partial^2 U}{\partial r_{\chi}^i \partial r_{\zeta}^j} \quad (9)$$

Clearly this is always symmetric and also positive semi-definite when computed for the minimized states. Its eigenvalues can therefore be only positive or zero, the latter originating from the symmetries of the system. We diagonalize the Hessian matrix using the LAPACK package [54] to obtain the normal modes of vibrations. This allows us to compute $S_{\text{glass}}^{\text{harm}}$ in terms of the normal modes as follows [55],

$$S_{\text{glass}}^{\text{harm}} = \left\langle \sum_{n=1}^{Nd} \{1 - \beta \hbar \omega_n\} \right\rangle_{\text{IS}} \quad (10)$$

with ω_n are the normal frequencies of vibrations. In figure 4, we plot this harmonic contribution as a function of effective temperature at various persistence times. As can be expected, the harmonic contribution is sensitive only to the variations in effective temperature but not the persistence time. In passive glass formers, this harmonic contribution usually plays the dominant role and the anharmonic contribution is almost always neglected in comparison [41]. We find this to be in stark contrast to active systems where the anharmonic contribution can become significant with activity and must be therefore included for the correct estimation of configurational entropy. This is discussed next.

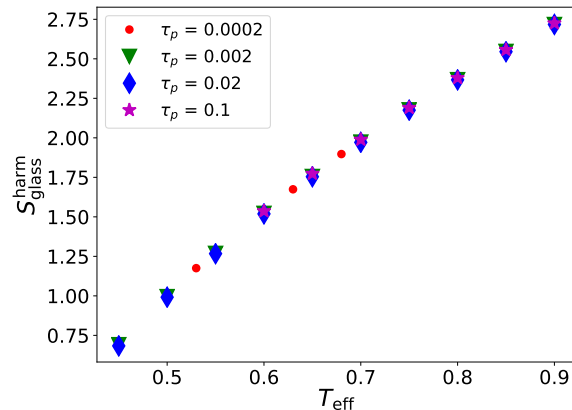


FIG. 4. Harmonic component of glass entropy as a function of T_{eff} . It is sensitive only to the effective temperature as can be expected from Eq. 10.

3. Anharmonic contribution to the glass entropy

In order to calculate the anharmonic glass entropy $S_{\text{glass}}^{\text{anh}}$ [55], we made use of the anharmonic energy E_{anh} which is the difference between the total energy and the harmonic energy. The anharmonic contribution $S_{\text{glass}}^{\text{anh}}$ can be calculated using the relation,

$$S_{\text{glass}}^{\text{anh}} = \int_0^{T_{\text{eff}}} \frac{dT'_{\text{eff}}}{T'_{\text{eff}}} \frac{\partial E_{\text{anh}}(T'_{\text{eff}})}{\partial T'_{\text{eff}}} \quad (11)$$

where, the integral in the equation 11 is solved by fitting $E_{\text{anh}}(T_{\text{eff}})$ with a polynomial of the form $E_{\text{anh}}(T_{\text{eff}}) = \sum_{m \geq 2} a_m T_{\text{eff}}^m$. This results in the simplified form of the above equation given by,

$$S_{\text{glass}}^{\text{anh}} = \sum_{m \geq 2} \frac{m}{m-1} a_m T_{\text{eff}}^{m-1} \quad (12)$$

here, the lower bound for the summation is chosen in such a way that, its heat capacity should go to zero at $T_{\text{eff}} = 0$. Figure 5 shows the temperature variation of the anharmonic entropy for various values of persistence

time. It is evident that the anharmonic contribution becomes negatively larger with increasing persistence time at any given effective temperature. In the following section we compute the total glass entropy.

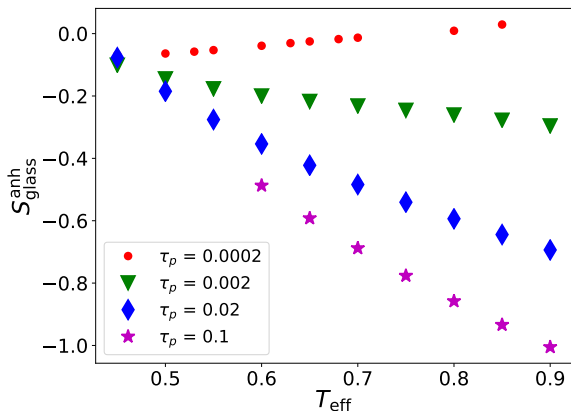


FIG. 5. Anharmonic contribution to the glass entropy as a function of T_{eff} . For a better representation we have shifted the curves for $\tau_p = 0.002, 0.02$ and 0.1 along the vertical axis by 1.2, 3.2 and 3.9 respectively.

4. Total glass entropy

Having calculated the harmonic and anharmonic contributions to the glass entropy, we are now in a position to calculate the S_{glass} which is a sum of both the contributions [56, 57].

$$S_{\text{glass}} = S_{\text{glass}}^{\text{harm}} + S_{\text{glass}}^{\text{anh}} \quad (13)$$

Figure 6 shows the behavior of the total glass entropy as a function of effective temperature for different persistence times. At any fixed effective temperature, the variation in entropy with persistence time is entirely due to the anharmonic contribution $S_{\text{glass}}^{\text{anh}}$ that was computed earlier. This asserts the importance and non-trivial nature of anharmonic effects in active systems that was stressed earlier in this paper. The results discussed here will enable us to compute the configurational entropy that can be used to describe the relaxation time of our low temperature active liquid. This is the subject matter of the next section.

C. Generalized Adam-Gibbs relation in the self-propelled system

RFOT offers a rationalized view of AG theory based on the activated dynamics. This generalization describes the glass transition via a thermodynamic route that connects the relaxation time τ_α to the configurational en-

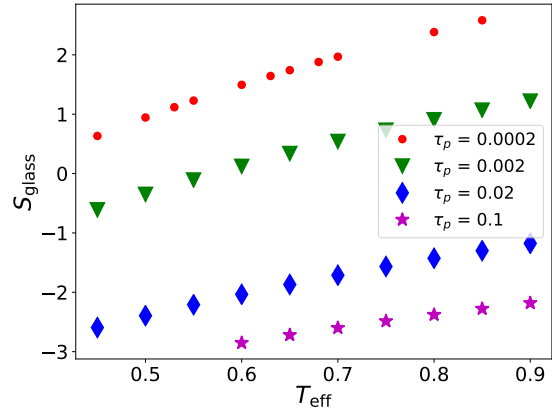


FIG. 6. Total glass entropy as a function of effective temperature at various levels of activity. Variation of glass entropy as a function of self-propulsion is entirely due to the anharmonic contributions discussed in the previous section.

trophy through the following relation [58, 59],

$$\tau_\alpha \sim \exp \left[\left(\frac{\Delta E}{T_{\text{eff}} S_c} \right)^\delta \right] \quad (14)$$

where ΔE is the energy barrier and δ is a non universal constant, both varying with the persistence time. This deviation from the actual AG theory ($\delta = 1$) was observed in previous studies [60]. The calculation of S_c is done using equation 5 that was discussed earlier and is shown in the figure 7 below. At a fixed τ_p , reducing T_{eff} leads to a reduction in the number of IS resulting in slower relaxation of the system (see figure 8) on the other hand, S_c grows with τ_p at a fixed T_{eff} . The latter has the effect of enhancing energy barrier height as a function of τ_p —an effect that is consistent with the growth of relaxation time with increasing persistence time at any fixed effective temperature (see figure 8). Table II shows the behavior of fitting parameters obtained from the generalized Adam-Gibbs relation obeyed by our data for different persistence times as shown in the figure 9.

τ_p	ΔE	δ
0.0002	1.280	1.503
0.002	4.520	2.095
0.02	6.129	3.636
0.1	8.041	4.605

TABLE II. The values of energy barrier and the degree of deviation from actual AG relation (δ) at various persistence times obtained as fitting parameters from equation 14.

The reader should note that the results reported here are obtained without recursing to a first order approximation of configurational entropy [27]. Further we went ahead and compute a static length scale ξ_s by a random pinning of particles and deduced an RFOT like scaling law between S_c and ξ_s . This is discussed below.

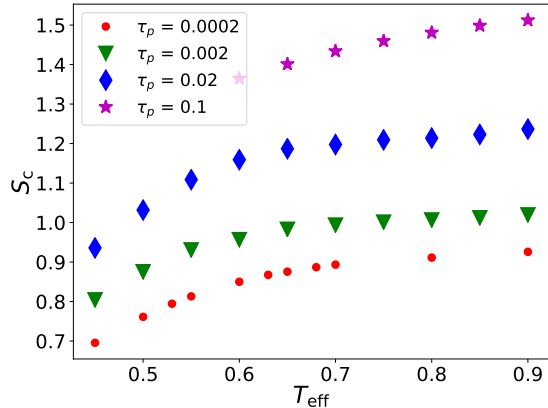


FIG. 7. Configurational entropy as a function of effective temperature at different values of τ_p . At a fixed τ_p , reducing T_{eff} reduces S_c . On the other hand, S_c increases as a function of τ_p at a fixed T_{eff} . For a better representation we have shifted the curves for $\tau_p = 0.002, 0.02$ and 0.1 along the vertical axis by $-3.20, -6.80$ and -8.00 respectively.

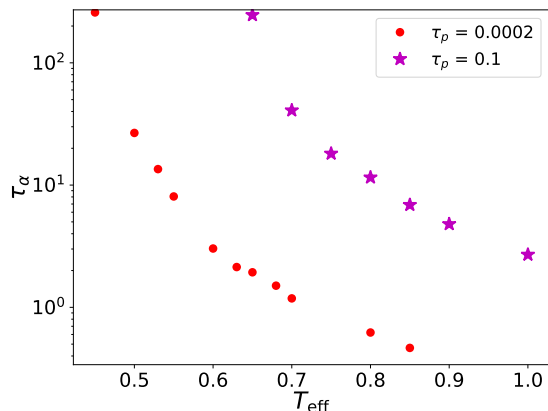


FIG. 8. Temperature variation of relaxation time at two different levels of activity. Note that $\tau_p = 0.002$ corresponds to the Brownian limit. It is evident that any fixed T_{eff} , relaxation time increases with τ_p .

IV. STATIC LENGTH SCALE AND THE CONFIGURATIONAL ENTROPY

The RFOT for the passive system suggests that liquid is composed of metastable regions called “mosaics” with a characteristic length scale ξ_s [24, 25, 61–63]. The reorganization of these mosaic regions depends on the energy barrier which scales as ξ_s^ψ [64, 65]. This directly provides a scaling relation between relaxation time and the length scale as follows,

$$\tau_\alpha \sim \exp\left(\frac{A \xi_s^\psi}{T_{\text{eff}}}\right) \quad (15)$$

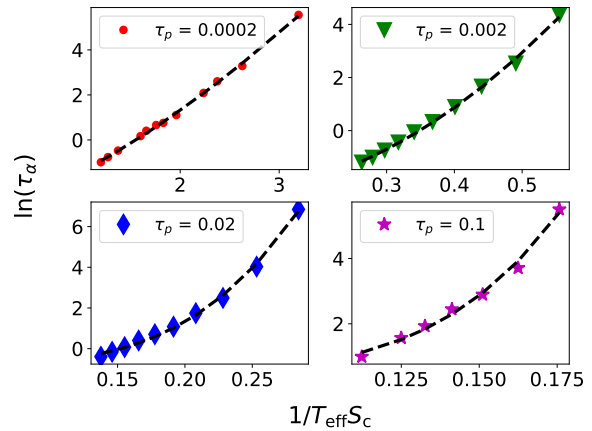


FIG. 9. Verification of generalized Adam-Gibbs relation for the various values of persistence time. Dashed line represents the scaling relation given in the eq. 14. The extracted ΔE and δ are given in table II.

where A is a constant. To extract the PTS static length scale ξ_s for self-propelled system we randomly choose particles in a steady state configuration and pin them such that they are distributed throughout the simulation region without any bias [66, 67]. Figure 10 shows such configurations with a pinning concentrations $c = 0.16, 0.25$ and 0.35 (from top to bottom). Using these pinned configurations as an initial state, we perform the dynamics for different T_{eff} and τ_p . All the runs are long enough to make sure that the self part of the overlap function (see eq. 17) decays to zero. The simulations are carried out for different pinning concentration. However, it should be noted that for each persistence time, at the low effective temperatures it is increasingly difficult to equilibrate the system as c becomes larger. We calculate the overlap functions between the configurations $\mathbf{r}_i(t)$ and $\mathbf{r}_j(t)$ which facilitate the extraction of length scale as follows [67–69].

$$Q(t) = \frac{1}{N - N_p} \left[\left\langle \sum_{i,j=1}^{N-N_p} \omega(|\mathbf{r}_i(t) - \mathbf{r}_j(0)|) \right\rangle \right] \quad (16)$$

where N_p is the number of pinned particles and the ω is a step function such that $\omega(x) = 1$ if $x < 0.30$ otherwise it is zero. Also, the self part of the overlap function reads as,

$$Q_s(t) = \frac{1}{N - N_p} \left[\left\langle \sum_{i=1}^{N-N_p} \omega(|\mathbf{r}_i(t) - \mathbf{r}_i(0)|) \right\rangle \right] \quad (17)$$

The figure 11 shows the behavior of total overlap function and its self part at an effective temperature $T_{\text{eff}} = 0.65$ and the persistence time $\tau_p = 0.002$. It is observed that, as the pinning concentration is increased, the relaxation

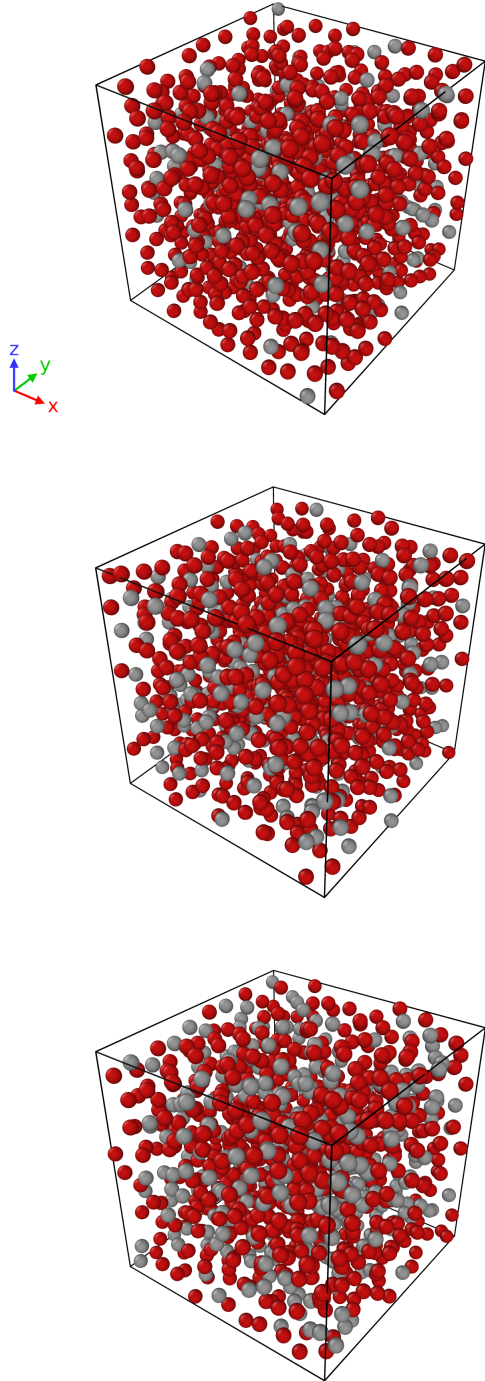


FIG. 10. Random pinning of the equilibrated configuration at an effective temperature $T_{\text{eff}} = 1.0$ and $\tau_p = 0.0002$ with a pinning concentrations of $c = 0.16, 0.25$ and 0.35 (from top to bottom). Here, the Grey particles are pinned while the red particles are unpinned.

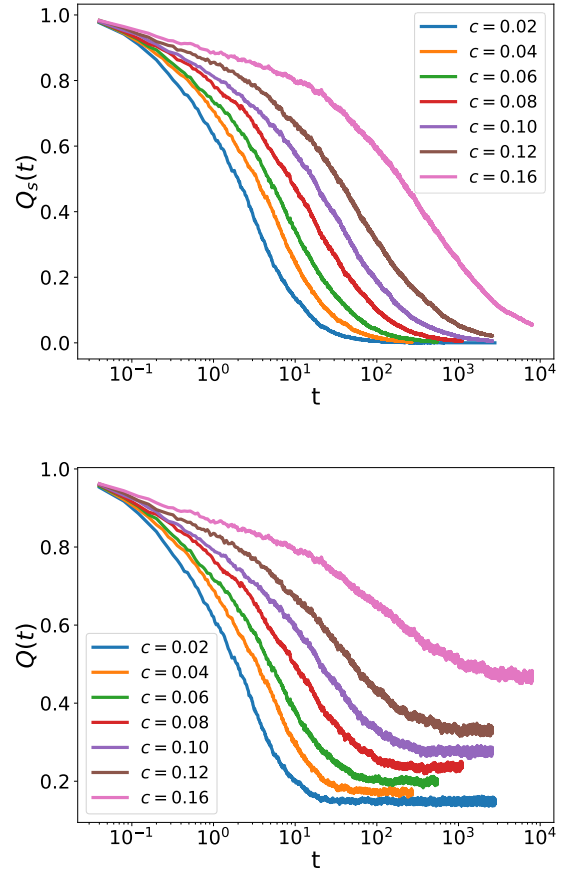


FIG. 11. The top and the bottom figures show the time decay of the self part and the total part of the overlap function respectively as a function of time for various pinning concentration at $T_{\text{eff}} = 0.65$ and $\tau_p = 0.002$. The asymptotic value of the total overlap function $Q_c(\infty)$ is measured when it saturates to a non-zero value.

time increases dramatically which makes the equilibration of the system a difficult task (see fig 11).

While the self part of the overlap function decays to zero, the total overlap function saturates at a non zero value in the asymptotic limit depending on pinning concentration. We denote this asymptotic value of the total overlap function as $Q_c(\infty)$, where the subscript c represents the pinning concentration. In order to extract the length from random pinning, we construct a quantity $Q_c(\infty) - Q_0(\infty)$ with $Q_0(\infty)$ being the asymptotic value of overlap function with zero pinning concentration [70]. The variation of the above constructed quantity as a function of average distance between the pinned particles $(c\rho)^{-1/3}$ is shown in the figure 12. Now, the length scale ξ_s is extracted as the value of $(c\rho)^{-1/3}$ corresponding to $Q_c(\infty) - Q_0(\infty) = 0.3$ at different T_{eff} . Figure 13 shows the validity of the scaling relation (eq. 15) for various persistence values. Values of A and the exponent ψ is given in the following table III.

Equations 14 and 15 enable us to deduce a scaling re-

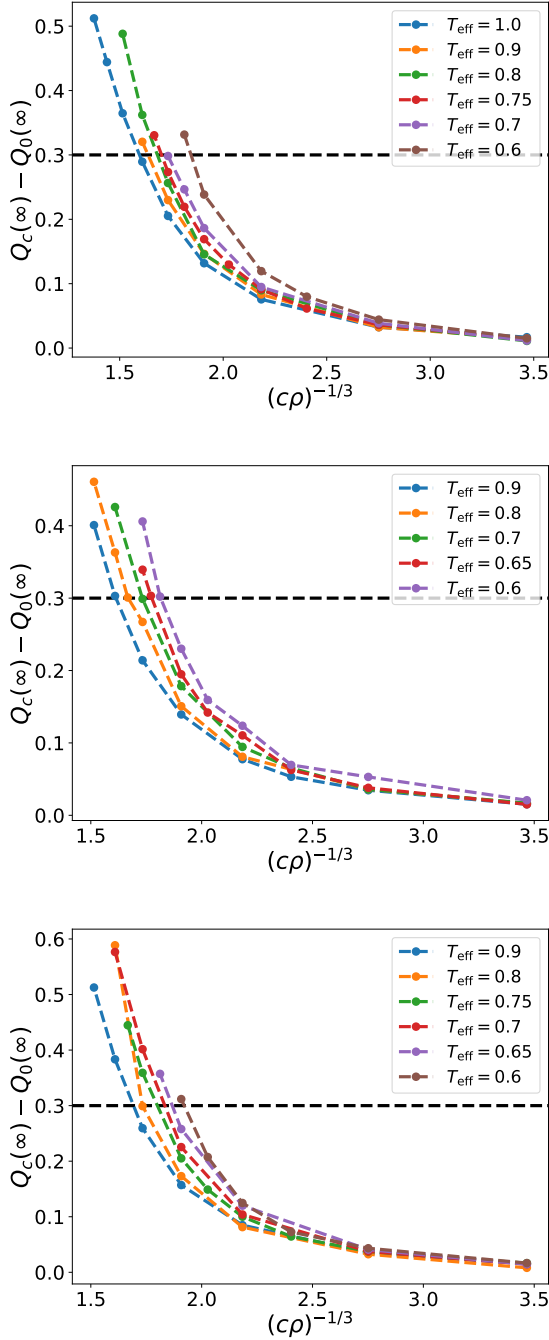


FIG. 12. The variation of difference between the asymptotic values of overlap function as a function of the average distance between the pinned particles. The shown plots are for $\tau_p = 0.0002, 0.002$ and 0.02 from top to bottom. In each case the length scale ξ_s is calculating value of $(c\rho)^{-1/3}$ corresponding to $Q_c(\infty) - Q_0(\infty) = 0.3$ which is marked by the horizontal dotted line.

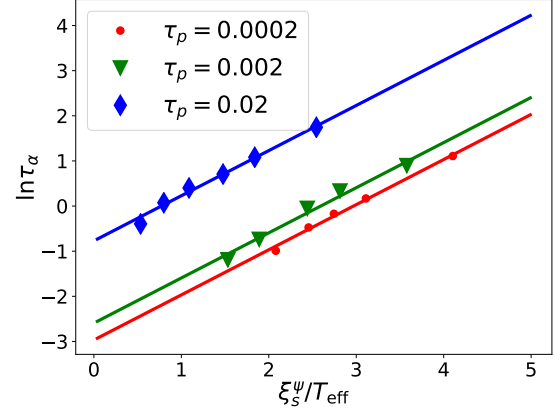


FIG. 13. The scaling law between the relaxation time τ_α with the mosaic length scale ξ_s for various values of τ_p . The solid curves represents the scaling law given by 15.

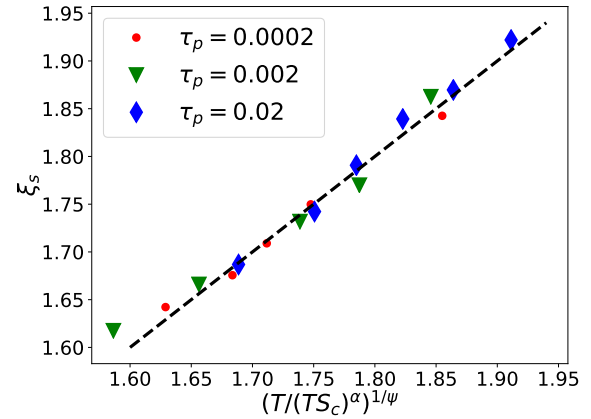


FIG. 14. Verification of the scaling law between S_c and the length scale ξ_s for various values of persistence time τ_p . Data for different τ_p collapsed on the master curve (dashed line) which is governed by the equation deduced (eq. 18).

τ_p	A	ψ
0.0002	0.574	2.382
0.002	0.304	3.141
0.02	0.007	8.859

TABLE III. The values of fitting parameters A and ψ as a function of persistence time obtained from the equation 15.

lation between S_c and ξ_s by eliminating τ_α given by

$$\xi_s = \left(\frac{\Delta E}{A} \right)^{1/\psi} \left(\frac{T_{\text{eff}}}{(T_{\text{eff}} S_c)^\delta} \right)^{1/\psi} \quad (18)$$

here, the effect of activity is to merely change the slope $\left(\frac{\Delta E}{A} \right)^{1/\psi}$. The validity of this scaling relation is presented in figure 14, where the data is collapsed on to a master curve (dashed line) that is given by the equation

18. Below we summarize our observations.

V. CONCLUSION

In this paper, we have provided an in detail calculation of the configurational entropy in the case of an athermal active glass former. Unlike passive liquids, the anharmonic contributions to configurational entropy are seen to be significant and also progressively increase with the degree of self-propulsion. The configurational entropy and relaxation time data for these self-propelled system satisfy the generalized for Adam-Gibbs relationship predicted by the random first order transition theory—an observation that has not been reported so far in the literature. Our data shows the effect of lowering the effective temperature at a fixed τ_p is to reduce the number of available states resulting in slower relaxation of the system. On the other hand, increasing τ_p at a fixed T_{eff} increases the energy barrier concomitant with activity enhancing

the glassy behavior in AOUP system. We established an exponential scaling relation between the relaxation time and the PTS length scale which along with the generalized AG relation enabled us to provide a direct relation between the PTS length scale ξ_s and the configurational entropy S_c in these active liquids. Our current work provides a thermodynamic way to understand the glassy dynamics of active systems. Our work can be used to study the physical systems such as Janus colloidal particles and the study of tracer particles in the bacterial suspension.

ACKNOWLEDGMENTS

We thank Ethayaraja Mani for discussions and comments on the manuscript. All simulations were done on the HPC-Physics cluster of our group and the AQUA super cluster of IIT Madras. Support from the core research grant SP20210716PHSERB008690 from SERB, Government of India, is gratefully acknowledged.

-
- [1] C. Dombrowski, L. Cisneros, S. Chatkaew, R. E. Goldstein, and J. O. Kessler, Self-concentration and large-scale coherence in bacterial dynamics, *Phys. Rev. Lett.* **93**, 098103 (2004).
- [2] T. Ishikawa, N. Yoshida, H. Ueno, M. Wiedeman, Y. Imai, and T. Yamaguchi, Energy transport in a concentrated suspension of bacteria, *Phys. Rev. Lett.* **107**, 028102 (2011).
- [3] N. Gravish, G. Gold, A. Zangwill, M. A. Goodisman, and D. I. Goldman, Glass-like dynamics in confined and congested ant traffic, *Soft matter* **11**, 6552 (2015).
- [4] A. Cavagna and I. Giardina, Bird flocks as condensed matter, *Annu. Rev. Condens. Matter Phys.* **5**, 183 (2014).
- [5] S. Hubbard, P. Babak, S. T. Sigurdsson, and K. G. Magnússon, A model of the formation of fish schools and migrations of fish, *Ecological Modelling* **174**, 359 (2004).
- [6] L. Berthier, Nonequilibrium glassy dynamics of self-propelled hard disks, *Phys. Rev. Lett.* **112**, 220602 (2014).
- [7] D. Gonzalez-Rodriguez, K. Guevorkian, S. Douezan, and F. Brochard-Wyart, Soft matter models of developing tissues and tumors, *Science* **338**, 910 (2012).
- [8] I. Theurkauff, C. Cottin-Bizonne, J. Palacci, C. Ybert, and L. Bocquet, Dynamic clustering in active colloidal suspensions with chemical signaling, *Phys. Rev. Lett.* **108**, 268303 (2012).
- [9] A. Sokolov and I. S. Aranson, Physical properties of collective motion in suspensions of bacteria, *Phys. Rev. Lett.* **109**, 248109 (2012).
- [10] A. Bricard, J.-B. Caussin, D. Das, C. Savoie, V. Chikkadi, K. Shitara, O. Chepizhko, F. Peruani, D. Saintillan, and D. Bartolo, Emergent vortices in populations of colloidal rollers, *Nature communications* **6**, 1 (2015).
- [11] N. Klongvessa, F. Ginot, C. Ybert, C. Cottin-Bizonne, and M. Leocmach, Active glass: Ergodicity breaking dramatically affects response to self-propulsion, *Physical review letters* **123**, 248004 (2019).
- [12] C. Bechinger, R. Di Leonardo, H. Löwen, C. Reichhardt, G. Volpe, and G. Volpe, Active particles in complex and crowded environments, *Reviews of Modern Physics* **88**, 045006 (2016).
- [13] R. Mandal, P. J. Bhuyan, P. Chaudhuri, C. Dasgupta, and M. Rao, Extreme active matter at high densities, *Nature communications* **11**, 1 (2020).
- [14] S. Henkes, K. Kostanjevec, J. M. Collinson, R. Sknepnek, and E. Bertin, Dense active matter model of motion patterns in confluent cell monolayers, *Nature communications* **11**, 1 (2020).
- [15] G. S. Redner, M. F. Hagan, and A. Baskaran, Structure and dynamics of a phase-separating active colloidal fluid, *Phys. Rev. Lett.* **110**, 055701 (2013).
- [16] L. Caprini, U. Marini Bettolo Marconi, and A. Puglisi, Spontaneous velocity alignment in motility-induced phase separation, *Physical review letters* **124**, 078001 (2020).
- [17] Y. Fily, S. Henkes, and M. C. Marchetti, Freezing and phase separation of self-propelled disks, *Soft matter* **10**, 2132 (2014).
- [18] A. Souslov, B. C. van Zuiden, D. Bartolo, and V. Vitelli, Topological sound in active-liquid metamaterials, *Nature Physics* **13**, 1091 (2017).
- [19] A. Czirók, A.-L. Barabási, and T. Vicsek, Collective motion of self-propelled particles: Kinetic phase transition in one dimension, *Physical Review Letters* **82**, 209 (1999).
- [20] Y. Fily and M. C. Marchetti, Athermal phase separation of self-propelled particles with no alignment, *Physical review letters* **108**, 235702 (2012).
- [21] E.-M. Schoetz, M. Lanio, J. A. Talbot, and M. L. Manning, Glassy dynamics in three-dimensional embryonic tissues, *Journal of The Royal Society Interface* **10**, 20130726 (2013).

- [22] T. Egami and C. W. Ryu, Why is the range of timescale so wide in glass-forming liquid?, *Frontiers in Chemistry* **8**, 579169 (2020).
- [23] P. G. Debenedetti and F. H. Stillinger, Supercooled liquids and the glass transition, *Nature* **410**, 259 (2001).
- [24] V. Lubchenko and P. G. Wolynes, Theory of structural glasses and supercooled liquids, *Annu. Rev. Phys. Chem.* **58**, 235 (2007).
- [25] T. R. Kirkpatrick and P. G. Wolynes, Connections between some kinetic and equilibrium theories of the glass transition, *Physical Review A* **35**, 3072 (1987).
- [26] T. R. Kirkpatrick, D. Thirumalai, and P. G. Wolynes, Scaling concepts for the dynamics of viscous liquids near an ideal glassy state, *Phys. Rev. A* **40**, 1045 (1989).
- [27] S. K. Nandi, R. Mandal, P. J. Bhuyan, C. Dasgupta, M. Rao, and N. S. Gov, A random first-order transition theory for an active glass, *Proceedings of the National Academy of Sciences* **115**, 7688 (2018).
- [28] R. Mandal, S. K. Nandi, C. Dasgupta, P. Sollich, and N. S. Gov, The random first-order transition theory of active glass in the high-activity regime, *Journal of Physics Communications* **6**, 115001 (2022).
- [29] E. Flenner, G. Szamel, and L. Berthier, The nonequilibrium glassy dynamics of self-propelled particles, *Soft matter* **12**, 7136 (2016).
- [30] R. Mandal, P. J. Bhuyan, M. Rao, and C. Dasgupta, Active fluidization in dense glassy systems, *Soft Matter* **12**, 6268 (2016).
- [31] Z. Preisler and M. Dijkstra, Configurational entropy and effective temperature in systems of active brownian particles, *Soft matter* **12**, 6043 (2016).
- [32] J. Deseigne, O. Dauchot, and H. Chaté, Collective motion of vibrated polar disks, *Physical review letters* **105**, 098001 (2010).
- [33] F. Ginot, I. Theurkauff, D. Levis, C. Ybert, L. Bocquet, L. Berthier, and C. Cottin-Bizonne, Nonequilibrium equation of state in suspensions of active colloids, *Physical Review X* **5**, 011004 (2015).
- [34] N. Koumakis, C. Maggi, and R. Di Leonardo, Directed transport of active particles over asymmetric energy barriers, *Soft matter* **10**, 5695 (2014).
- [35] G. Szamel, E. Flenner, and L. Berthier, Glassy dynamics of athermal self-propelled particles: Computer simulations and a nonequilibrium microscopic theory, *Phys. Rev. E* **91**, 062304 (2015).
- [36] U. M. B. Marconi and C. Maggi, Towards a statistical mechanical theory of active fluids, *Soft matter* **11**, 8768 (2015).
- [37] E. Fodor, C. Nardini, M. E. Cates, J. Tailleur, P. Visco, and F. van Wijland, How far from equilibrium is active matter?, *Phys. Rev. Lett.* **117**, 038103 (2016).
- [38] R. Mannella and V. Palleschi, Fast and precise algorithm for computer simulation of stochastic differential equations, *Phys. Rev. A* **40**, 3381 (1989).
- [39] W. Kob and H. C. Andersen, Testing mode-coupling theory for a supercooled binary lennard-jones mixture i: The van hove correlation function, *Phys. Rev. E* **51**, 4626 (1995).
- [40] A. Banerjee, S. Sengupta, S. Sastry, and S. M. Bhattacharyya, Role of structure and entropy in determining differences in dynamics for glass formers with different interaction potentials, *Physical review letters* **113**, 225701 (2014).
- [41] L. Berthier, M. Ozawa, and C. Scalliet, Configurational entropy of glass-forming liquids, *The Journal of chemical physics* **150**, 160902 (2019).
- [42] F. Sciortino, W. Kob, and P. Tartaglia, Inherent structure entropy of supercooled liquids, *Physical Review Letters* **83**, 3214 (1999).
- [43] B. Coluzzi, G. Parisi, and P. Verrocchio, Lennard-jones binary mixture: a thermodynamical approach to glass transition, *The Journal of Chemical Physics* **112**, 2933 (2000).
- [44] T. S. Ingebrigtsen, A. A. Veldhorst, T. B. Schröder, and J. C. Dyre, Communication: The rosenfeld-tarazona expression for liquids' specific heat: A numerical investigation of eighteen systems, *The Journal of Chemical Physics* **139**, 171101 (2013).
- [45] P. Das and S. Sastry, Crossover in dynamics in the kob-andersen binary mixture glass-forming liquid, *Journal of Non-Crystalline Solids: X* **14**, 100098 (2022).
- [46] S. Sastry, The relationship between fragility, configurational entropy and the potential energy landscape of glass-forming liquids, *Nature* **409**, 164 (2001).
- [47] S. Sastry, Inherent structure approach to the study of glass-forming liquids, *Phase Transitions* **75**, 507 (2002).
- [48] A. Heuer, Exploring the potential energy landscape of glass-forming systems: from inherent structures via metabasins to macroscopic transport, *Journal of Physics: Condensed Matter* **20**, 373101 (2008).
- [49] S. Sastry, P. G. Debenedetti, F. H. Stillinger, T. B. Schröder, J. C. Dyre, and S. C. Glotzer, Potential energy landscape signatures of slow dynamics in glass forming liquids, *Physica A: Statistical Mechanics and its Applications* **270**, 301 (1999).
- [50] J. R. Shewchuk *et al.*, An introduction to the conjugate gradient method without the agonizing pain (1994).
- [51] J. Nocedal and S. J. Wright, Conjugate gradient methods, *Numerical optimization*, 101 (2006).
- [52] S. Wright, J. Nocedal, *et al.*, *Numerical optimization*, Springer Science **35**, 7 (1999).
- [53] S. Karmakar, E. Lerner, and I. Procaccia, Athermal non-linear elastic constants of amorphous solids, *Physical Review E* **82**, 026105 (2010).
- [54] E. Anderson, Z. Bai, C. Bischof, L. S. Blackford, J. Demmel, J. Dongarra, J. Du Croz, A. Greenbaum, S. Hammarling, A. McKenney, *et al.*, *LAPACK users' guide* (SIAM, 1999).
- [55] F. Sciortino, Potential energy landscape description of supercooled liquids and glasses, *Journal of Statistical Mechanics: Theory and Experiment* **2005**, P05015 (2005).
- [56] L. Angelani and G. Foffi, Configurational entropy of hard spheres, *Journal of Physics: Condensed Matter* **19**, 256207 (2007).
- [57] S. Sastry, Evaluation of the configurational entropy of a model liquid from computer simulations, *Journal of Physics: Condensed Matter* **12**, 6515 (2000).
- [58] J.-P. Bouchaud and G. Biroli, On the adam-gibbs-kirkpatrick-thirumalai-wolynes scenario for the viscosity increase in glasses, *The Journal of chemical physics* **121**, 7347 (2004).
- [59] M. Ozawa, C. Scalliet, A. Ninarello, and L. Berthier, Does the adam-gibbs relation hold in simulated supercooled liquids?, *The Journal of chemical physics* **151**, 084504 (2019).
- [60] S. Sengupta, S. Karmakar, C. Dasgupta, and S. Sastry, Adam-gibbs relation for glass-forming liquids in two,

- three, and four dimensions, *Physical review letters* **109**, 095705 (2012).
- [61] T. R. Kirkpatrick, D. Thirumalai, and P. G. Wolynes, Scaling concepts for the dynamics of viscous liquids near an ideal glassy state, *Physical Review A* **40**, 1045 (1989).
- [62] G. Biroli and J.-P. Bouchaud, The random first-order transition theory of glasses: A critical assessment, *Structural Glasses and Supercooled Liquids: Theory, Experiment, and Applications*, 31 (2012).
- [63] T. R. Kirkpatrick and D. Thirumalai, Colloquium: Random first order transition theory concepts in biology and physics, *Rev. Mod. Phys.* **87**, 183 (2015).
- [64] F. W. Starr, J. F. Douglas, and S. Sastry, The relationship of dynamical heterogeneity to the adam-gibbs and random first-order transition theories of glass formation, *The Journal of chemical physics* **138**, 12A541 (2013).
- [65] S. Karmakar, C. Dasgupta, and S. Sastry, Growing length and time scales in glass-forming liquids, *Proceedings of the National Academy of Sciences* **106**, 3675 (2009).
- [66] L. Berthier and W. Kob, Static point-to-set correlations in glass-forming liquids, *Physical Review E* **85**, 011102 (2012).
- [67] S. Chakrabarty, R. Das, S. Karmakar, and C. Dasgupta, Understanding the dynamics of glass-forming liquids with random pinning within the random first order transition theory, *The Journal of chemical physics* **145**, 034507 (2016).
- [68] N. Lačević, F. W. Starr, T. Schröder, and S. C. Glotzer, Spatially heterogeneous dynamics investigated via a time-dependent four-point density correlation function, *The Journal of chemical physics* **119**, 7372 (2003).
- [69] U. K. Nandi, P. Patel, M. Moid, M. K. Nandi, S. Sengupta, S. Karmakar, P. K. Maiti, C. Dasgupta, and S. Maitra Bhattacharyya, Thermodynamics and its correlation with dynamics in a mean-field model and pinned systems: A comparative study using two different methods of entropy calculation, *The Journal of Chemical Physics* **156**, 014503 (2022).
- [70] P. Charbonneau and G. Tarjus, Decorrelation of the static and dynamic length scales in hard-sphere glass formers, *Physical Review E* **87**, 042305 (2013).